DOI 10.1007/s10812-024-01799-5
Journal of Applied Spectroscopy, Vol. 91, No. 4, September, 2024 (Russian Original Vol. 91, No. 4, July–August, 2024)

SPECTROSCOPIC STUDIES ON PLANT EXTRACT MEDIATED ZnO NANOPARTICLES AS A POTENTIAL CYTOTOXIC AGENT

B. T. Delma,[a,*] M. Antilin Princela,[a] Y. Subbareddy,[b,*] M. Anitha Malbi,[a] S. Lizy Roselet,[a] M. Shirly Treasa,[a] and M. C. Rao[c,*]

UDC 543.42;620.3

Plants play an important role in nanoparticle preparation because they are easily accessible, environmentally friendly, and inexpensive. In this study, we used an ethanolic extract of Mangifera indica seed as a reducing and stabilising agent to create zinc oxide (ZnO) nanoparticles (NPs). The ZnO NPs were examined using characterization techniques such as UV-Vis, Fourier transform infrared (FT-IR), X-ray diffraction (XRD), scanning electron microscopy (SEM), and transmission electron microscopy (TEM). The interaction of phytochemical constituents from plant extracts providing the biological reduction of zinc metal ions to ZnO had been identified by the UV-visible absorption studies. According to the FT-IR results, metal oxides exhibited interatomic vibration-driven absorption in the fingerprint area below 1000 cm^{-1}. Particles appeared to be crystalline and also a rice-grain shape of ZnO NPs was confirmed by XRD, SEM, and TEM, respectively. In addition, the cytotoxic effect of ZnO NPs was checked using the SKMEL-28 cell line, showing an IC50 value of 32.686 μg/mL in the SKMEL-28 cell line, and 49.011 μg/mL in the typical L6 cell line. Furthermore, the synthesized NPs were subjected to (AO/EB) double staining approach to examine the apoptotic activity. The acridine orange/ethidium bromide method made strong evidence for demonstrating chromatin condensation and membrane blebbing.

Keywords: *Mangifera indica seed, ZnO NPs, UV-Visible, FT-IR, cytotoxicity, apoptotic activity.*

Introduction. Cancer detection and its treatment are well revolutionized in the area of important applications of nanotechnology. Especially nanomedicine is a fast grow research area in the field of medicine. Owing to the tiny size and high surface area to volume ratio, nanoparticles (NPs) exhibit outstanding biological activity. A number of methods have been implemented to synthesize NPs such as physical, chemical, and biological processes [1]. Of these, the physical and chemical methods have an impact by producing numerous by-products, which are highly harmful to society, is possibly more expensive, and is a process that needs high temperature and pressure [2]. Conversely, the biological approach would be risk-free, manageable, toxicology-controlled, eco-friendly and environmentally acceptable, as plants are widely accessible, inexpensive, renewable, and nontoxic [3]. Numerous attempts were made to exhibit the efficiency of zinc towards biological studies — for instance, various zinc complexes [4], metal-doped zinc oxide (ZnO) NPs [5], zinc sulphate [6], zinc metal salts [7], zinc ferrite NPs [8] and so on. However, ZnO NPs, have strong antibacterial, antifungal, antidiabetic, anti-inflammatory, antioxidant and rapid wound-healing tendencies. In addition, ZnO NPs have been used in various industries for the fabrication of nano-optical devices, nano-electrical devices, and modified electrode fabrication [9] as well as antibacterial food packaging sheets [10]. The naturally available plants have been used as a precursor for nanoparticle synthesis. In addition, the phytochemical constituents from the plant extract are the best capping and reducing agents in biology [11].

In this scenario, ZnO NPs were obtained from a variety of plant extracts [12, 13], which have been utilized to treat cancer in several cell lines, including the A549 cell line, human hepatocarcinoma (HepG2) cell line, human colorectal epithelial

*To whom correspondence should be addressed.

[a]Department of Chemistry, Holy Cross College (Autonomous), Nagercoil, Tamil Nadu, India; (Affiliated to Manonmaniam Sundaranar University, Abishekapatti, Tirunelveli, Tamil Nadu, India); email: delma.chem5@gmail.com; [b]Department of Chemistry, Andhra Loyola College (Autonomous), Vijayawada, India; email: ysrdpalc@gmail.com; [c]Department of Physics, Andhra Loyola College (Autonomous), Vijayawada, India; email: raomc72@gmail.com. Abstract of article is published in Zhurnal Prikladnoi Spektroskopii, Vol. 91, No. 4, p. 611, July–August, 2024.

adenocarcinoma (Caco-2) cell line, and breast cancer cell line (MCF-7) [14]. The deadliest diseases, such as AIDS, hepatitis, and malignancies could be treated and prevented with the use of plant-derived therapeutic substances [15]. The *Mangifera indica* seed has been historically utilized by rural people as an antibiotic against the stomach infections of newborns. Additionally, it has an appealing profile of essential amino acids and lipids (6–16%) and is an excellent source of carbohydrates (58–80%) and protein (6–13%). It is also high in oleic and stearic acids. Due to its strong antioxidant capacity, it has been found to have an anticancer effect against breast and colon cancer and antibacterial activity against Gram-positive and Gram-negative bacteria. Its high tannin content plays a significant role in antidiarrheal effects [16]. Generally, the *Mangifera indica* seeds were discarded as waste material in food production industries. However, our interest is to utilize these bioactive Mangifera indica seeds, for the preparation of ZnO NPs. As far as we are aware, there are no reports available regarding the synthesis of ZnO NPs via *Mangifera indica* ethanolic seed extract. Hence, the ethanolic seed extract of *Mangifera indica* is a brand-new and novel reagent for making ZnO NPs. Thus, the eco-friendly ethanolic seed extract of *Mangifera indica*, with its unique and low-cost capping as well as reducing agent for the synthesis of ZnO NPs, was utilized. In order to find the biological activity of newly prepared ZnO NPs, the cytotoxic effect on SKMEL-28 cell line was evaluated. The ZnO NPs derived from the *Mangifera indica* seed extract exhibited excellent biological activity as well as an admirable cytotoxic effect towards the SKMEL-28 cell line.

Materials and Methods. *Mangifera indica* seeds were collected in Marthandam, India. The seeds were then broken up into small pieces and allowed to dry for 12–14 days in the shade at room temperature before being mechanically blended. A total of 5 g of powdered *Mangifera indica* seeds were taken in a clean cloth and neatly packed. The packed sample was placed in a thimble and then extracted with 500 mL of ethanol as a solvent using a Soxhlet extractor. The extraction was completed in 10–15 h at a regulated temperature of 60^{o}C. The extract was collected, concentrated, and stored in an airtight container for further use. ZnO NPs were prepared using a zinc nitrate solution purchased from Merck, India. A total of 1 mL of the *Mangifera indica* seed extract was added dropwise into 10 mL of 0.1 M zinc nitrate solution to which 1 mL of NaOH solution was later added. While maintaining a temperature of 60^{o}C, the reaction mixture was stirred continuously till the colour of the solution changed to white. It became yellow after 1 day and was then centrifuged for five minutes at 15,000 rpm. Subsequently, the supernatant liquid was discarded and the precipitate was collected. After the synthesis of ZnO NPs from *Mangifera indica* seed extract, it was filtered using Whatman No. 1 filter paper and stored in an airtight container for later use.

The synthesized ZnO NPs were confirmed by UV-Visible spectrophotometer (Shimadzu UV-1800). The functional groups present in the ZnO NPs were detected by FT-IR (Shimadzu FTIR 84005) analysis. The crystalline nature of ZnO NPs can be studied by XRD (Shimadzu XRD 6000, Japan) and also the average grain size of the ZnO NPs was calculated using the Scherrer's equation. The surface morphology and components present in the ZnO NPs were analyzed by SEM with EDAX (JEOL JSM 6390 Scanning Electron Microscope equipped with energy dispersive spectroscopy (EDAX) capability, Japan). The size and shape of the ZnO NPs were analyzed by using TEM (JEOL JEM-2100F Field Emission Electron Microscope).

Both the SK-MEL-28 and regular L6 cell lines were purchased from the National Centre for Cell Sciences (NCCS) in Pune, India and grown in Dulbecco's modified Eagles medium (DMEM; HiMedia). The cell lines were cultured in a 25-cm^2 tissue culture flask with DMEM supplemented with 10% FBS, L-glutamine, sodium bicarbonate, and an antibiotic solution made up of penicillin (100 U/mL), streptomycin (100 g/mL), and amphotericin B (2.5 g/mL). Cultured cell lines were incubated at 37^{o}C in a humidified 5% CO_2 incubator (Galaxy® 170 Eppendorf, Germany). Using an inverted phase-contrast microscope to observe the cells up close first hand, the 3-(4,5-dimethylthiazol-2-yl)-2,5-diphenyltetrazolium bromide (MTT) test method was used to gauge the viability of the cells. A trypsinized two-day-old confluent monolayer of cells was sown in 96-well tissue culture plates at a density of 5×10^4 cells per well. The cells were then incubated at 37^{o}C on a humidified 5% CO_2 incubator. These plates were exposed to ZnO NPs at concentrations of 6.25, 12.5, 25, 50, and 100 g/mL for cancer cells and 6.25, 12.5, 25, 50, and 100 g/mL for L6 normal cells to investigate the cytotoxic effects. After 24 h of incubation, cells were washed with a phosphate buffer before the addition of 100 mL of MTT solution to all 96 wells and incubated for 2–3 h at 37^{o}C. Following the incubation, the crystals formed by the MTT solution were dissolved in 100 L of DMSO in each well, and the entire plate was agitated for 10 to 15 min to produce color. To determine the viability of the cell, the plate was then read using the spectrophotometric method at 570 nm using the below equation

$$\text{Cell viabilty} = \frac{\text{Optical density of ZnO nanoparticle}}{\text{Optical density of control}} \times 100\%.$$

For the morphological identification of apoptotic and necrotic cells, the DNA-binding dyes acridine orange (AO) and ethidium bromide (EB) (Sigma, USA) were employed. When AO intercalates into a double-stranded nucleic acid, it exhibits green fluorescence and is absorbed by both living and dead cells (DNA). Only nonviable cells may absorb EB, which then emits red fluorescence by intercalation into DNA. Cells were treated with test sample IC50 concentrations and then incubated in a CO_2 incubator for 24 h before being rinsed with cold PBS and stained with a combination of AO and EB for 10 min at room temperature. The stained cells were rinsed twice with 1X PBS before being viewed using a fluorescent microscope with a blue filter (Olympus CKX41 with Optika Pro5 camera).

Results and Discussion. *UV-visible spectral studies.* The analytical technique measures the number of discrete wavelengths of light that are absorbed or transmitted through a sample in comparison to the reference sample. The synthesized ZnO NPs were analyzed using UV-Visible spectrophotometer. The interaction of phytochemical constituents from plant extracts providing the biological reduction of zinc metal ions to ZnO was proven by the absorption band of UV-visible spectrum. In this scenario, the broad peak obtained at 325 nm (Fig. 1) confirms the formation of the produced ZnO NPs. Furthermore, the color of ZnO NPs changes from white to yellow [17] owing to the surface plasmon resonance band. Earlier reports suggested that the formation of ZnO NPs using *Ulva lactuca* seaweed extract [18], *Cassia alata* extract [19] and *Scutellaria baicalensis* Root extracts [20] has shown similar peaks, making strong evidence for the above data.

FT-IR studies. The FT-IR is a useful tool for understanding local structural changes in the materials. The nature of bonding and different functional groups in the prepared sample can be identified using vibrational frequencies. The bands appeared at 3431.98, 2925.07, 2853.64, 2354.48, 1719.34, 1541.19, 1476.64, 1334.64, 1227.06, 1042.02, and 870.76 cm^{-1} in the FT-IR spectrum (Fig. 2a) for the ethanol extract of the *Mangifera indica* seed. The –OH stretching vibration of phenols is represented by the band at 3431.98 cm^{-1}, and the C–H stretching vibration of primary and secondary amines is indicated by the bands at 2925.07 and 1334 cm^{-1}. The identification of bands at 2853.64, 1541.19, 1334.64, 1227.06 cm^{-1}, and C–H bending of aromatic C=C and alcohols, respectively, showed the presence of polyphenolic chemicals [21]. The aromatic group's C–O and C–S stretching were represented by the band at 870.76 cm^{-1} [22]. A distinctive band at 1042.02 cm^{-1} indicates O–C–C stretching, whereas the aromatic ring's stretching vibration shows at 1476.64 cm^{-1}. The flavonoids, terpenoids, and tannins found in the seed extract are primarily responsible for these observed peaks. Gallic acid, gallotannins, ellagic acid, Xanthones (Mangiferin), methyl gallate, digallic acid, gallotannin, and glucogallin are among the polyphenols abundant in the ethanolic extract of the *Mangifera indica* seed [23].

The stretching vibration of the aromatic ring for ZnO NPs (Fig. 2b) emerges at 1449 cm^{-1} and the O–H scissoring deformation of an aromatic ring is shown at 1326 cm^{-1}. Stretching of the C–H axis is responsible for the band at 1360 cm^{-1}. At 1207 and 1180 cm^{-1}, respectively, the distinctive bands of C–O aromatic stretching and C–O–C asymmetric stretching are seen. A distinctive band at 1043 cm^{-1} can be used to detect O–C–C stretching. The C–O stretching of alcohols is represented by the vibrational bands seen at 838 cm^{-1}. Figure 2b displays the spectrum which was measured in terms of transmittance percentage at various wavelengths. According to the FT-IR results, metal oxides exhibit interatomic vibration-driven absorption in the fingerprint area below 1000 cm^{-1}. The plant extract's soluble components may have served as a coating agent to prevent the aggregation of NPs in solution and to significantly contribute to their synthesis and structural development [24].

XRD analysis. X-ray diffraction (XRD) is a powerful and proven technique for investigating the structural properties of materials. The XRD analysis was performed to investigate the prepared material as to whether it is amorphous or crystalline in nature. Figure 3 shows the XRD pattern of ZnO NPs. The 2θ values of ZnO NPs found at 31.8979, 34.5163, 36.3649, 47.6640, 56.6873, 62.9709, 66.5177, 68.0509, 69.2007, and 77.0027° correspond to the JCPDS file no. 361451 and are indexed as the zinc oxide wurtzite structure. The 2θ values correlate with the planes (100), (002), (101), (102), (110), (103), (200), (112), (201), and (202) [25]. The average grain size of the ZnO NPs is estimated using the Debye–Scherrer's formula:

$$D = \frac{0.9\lambda}{\beta \cos \theta} \times 100\% \ ,$$

where D is the crystal size, λ is the wavelength of the X-rays, θ is the Bragg's angle in radians, and β is the full width at half the maximum of the peak in radians. The average grain size of the ZnO NPs is found to be 20.46 nm.

SEM–EDAX studies. Scanning electron microscope (SEM) is one of the most widely used instrumental methods for the examination and analysis of micro and nanoparticle imaging characterization of materials. This instrument may also be used in conjunction with other related techniques of energy-dispersive X-ray microanalysis (EDAX) for the determination

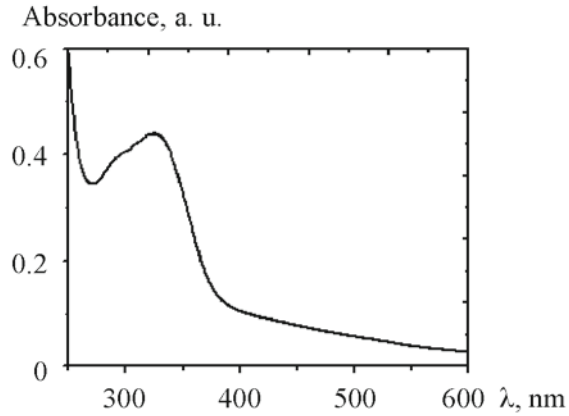

Fig. 1. UV-Visible spectrum of ZnO NPs.

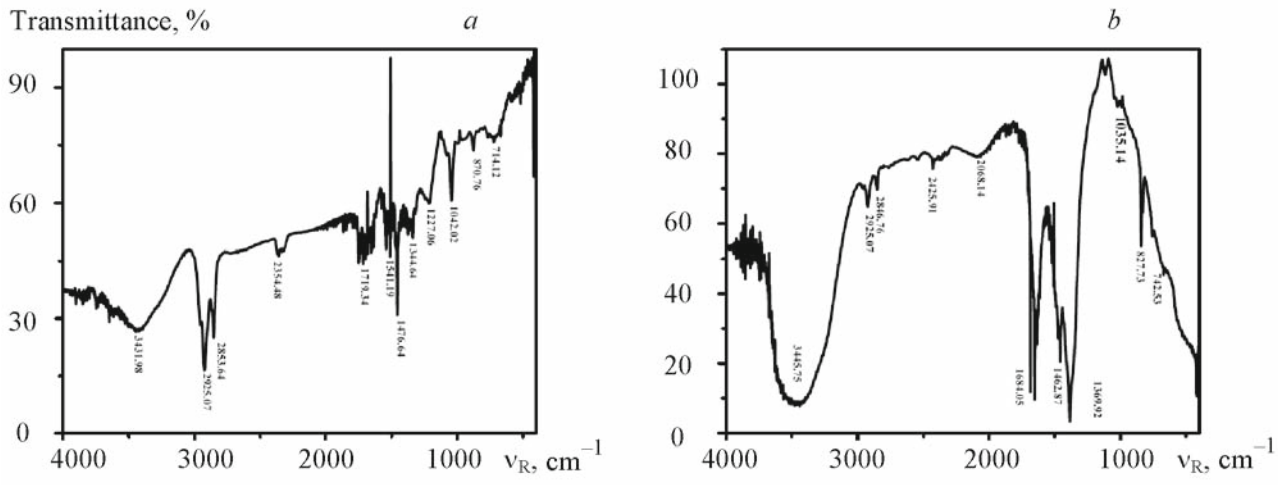

Fig. 2. FT-IR spectrum of *Mangifera indica* seed extract (a) and ZnO NPs (b).

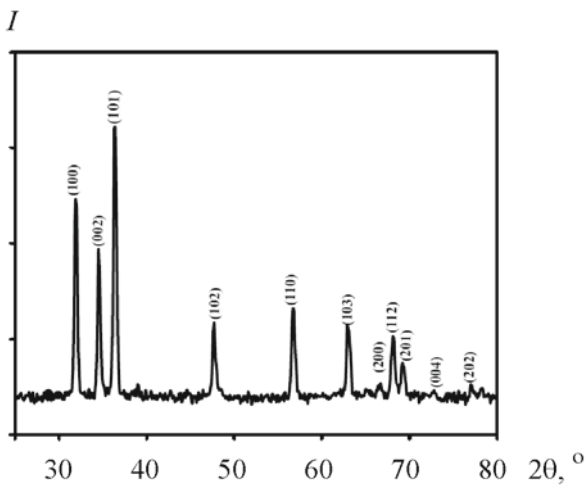

Fig. 3. XRD pattern of ZnO NPs.

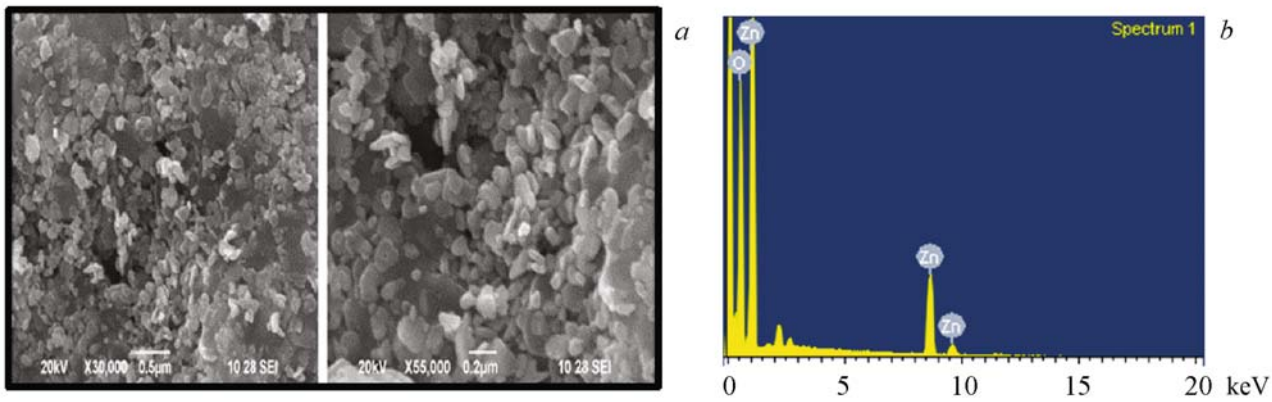

Fig. 4. (a) SEM images of ZnO NPs at different resolutions, (b) EDAX pattern of ZnO NPs.

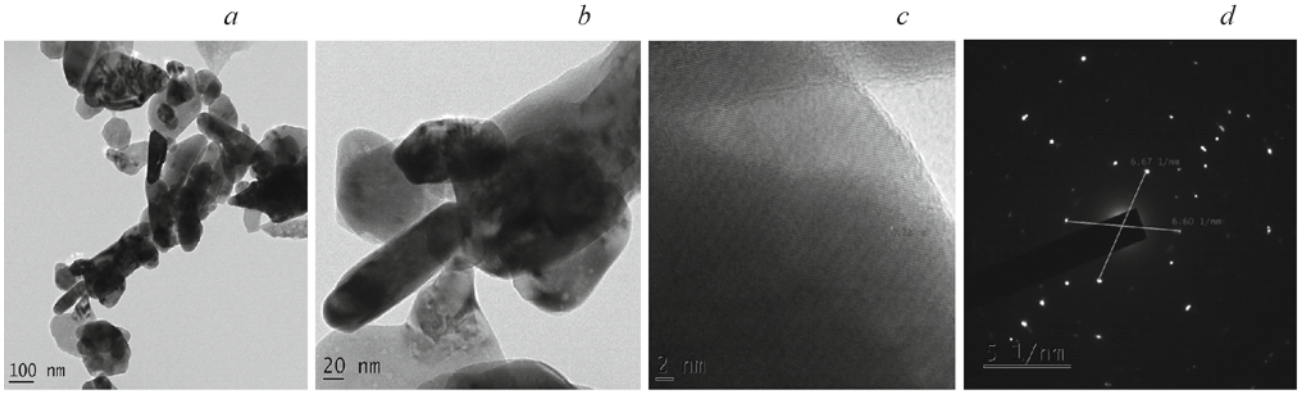

Fig. 5 HR-TEM micrographs of ZnO NPs taken at different magnifications (a) 50 nm, (b) 20 nm, (c) HR-TEM images of ZnO NPs showing the lattice spacing of 0.22 nm, (d) electron diffraction pattern of ZnO NPs.

of the composition or orientation of individual crystals or features. The SEM images (Fig. 4a) of the ZnO NPs at different resolutions possess rice-like morphology [26] and the average grain size of the nanoparticle is found to be 43.44 nm. EDAX spectrum (Fig. 4b) shows the elemental composition of ZnO NPs, revealing that no impurities are present in the compound. The weight percentage of zinc (Zn) and oxygen (O) in ZnO NPs are 54.37 and 45.63%, respectively [27].

TEM analysis. Transmission electron microscopy (TEM) is an analytical technique used to visualize the smallest structures in materials. The TEM image of the ZnO NPs (Fig. 5) shows the nanoparticles having a rice-like structure and it is similar to the SEM image. The length and diameter of the ZnO NPs are found to be 69.68 nm to 0.30 μm and 29.41 to 85.648 nm. The fringe spacing is 0.22 nm, corresponding to the (101) plane of ZnO NPs [28].

Cytotoxicity and apoptotic activity. The anticancer activity of the NPs depends on the cell line, concentration and exposure time. The cytotoxicity of the ZnO NPs in the SKMEL-28 cell line is determined by the MTT assay. It depends on the formation of Formazan crystal from yellow tetrazolium dye by mitochondrial succinate dehydrogenase enzyme. The percentage of cell viability is calculated in terms of the rate of Formazan crystals based on their optical density. Usually, ZnO NPs act as a good anticancer agent and has been proved by many *in vitro* studies to selectively kill cancer cells. In physiological conditions, ZnO NPs carry a positive charge, because they have an isoelectric point at pH 9–10, and the cancer cells have negative phospholipids. Hence, there is an electrostatic interaction that is maintained between the metal oxide NPs and cancer cells, which promotes the anti-cancer activity of the NPs [29].

The anticancer activity of the ZnO NPs (Fig. 6) is dose-dependent. Table 1 shows the concentration of ZnO NPs versus the percentage of cell viability against the SKMEL-28 cell line and L6 normal cell line by MTT assay. Concentrations

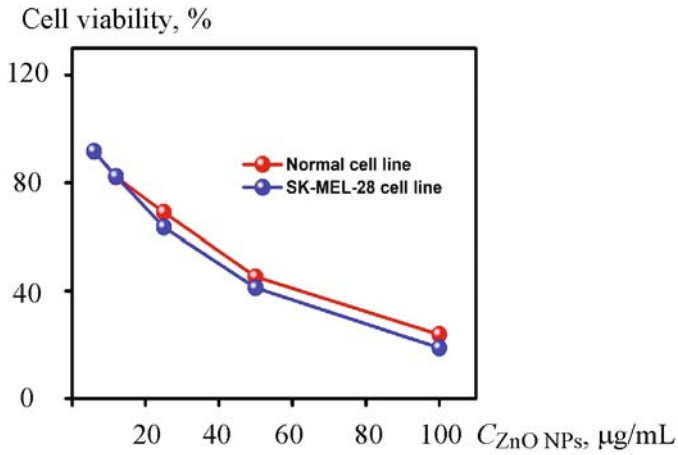

Fig. 6. Cytotoxic effect of ZnO NPs on the SKMEL-28 cell line.

TABLE 1. MTT Assay of ZnO NPs

ZnO NPs concentration, μg/mL	Cell viability, %	
	SK-MEL-28 cell line	L6 Normal cell line
6.25	91.76	91.66
12.5	82.35	82.14
25	63.52	69.04
50	41.17	45.23
100	18.82	23.8
IC50	32.68	49.01

such as 6.25, 12.5, 25, 50, and 100 μg/mL were used to check the anticancer activity of ZnO NPs against the tested cancer cell line. As the concentration increased, the cell viability continues to decrease, exhibiting the potent IC_{50} value (Table 1). It is evident that the IC_{50} value of ZnO NPs in the SKMEL-28 cell line is 32.686 μg/mL, while in the normal L6 cell line it is 49.011 μg/mL. These results show that ZnO NPs have less effect in normal cell lines and also affect the cancer cell line [30]. Moreover, a dose-response curve was drawn in terms of the concentration of ZnO NPs and cell viability as shown in Fig. 6. The curve indicates that the cell viability decreases based on the concentration of the ZnO NPs. At higher concentrations, the cell viability on the SKMEL-28 cell line showed better activity. However, the 50% growth of inhibition was exhibited at approximately 40 μg/mL, whereas at maximum concentrations, the growth of inhibition was around 20% [31]. Further, the calculation of cell viability in this study is reliable because we measured cell viability through triplicate testing responses. We plotted the percentage of cell viability versus the logarithmic concentration of ZnO NPs using a dose-response model and obtained sigmoidal curves using origin software (Fig. 7). These dose-response curves allowed us to determine the 50% minimum inhibitory concentration (IC_{50}) value for both the SKMEL-28 cell line and the normal cell line [32–34].

After the treatment of cancer cells with ZnO NPs, the changes that occurred were confirmed by fluorescent microscopic images shown in Fig. 8. In order to compare the microscopic images of normal cells and treated cancer cells, there may be a drastic change in the cancer cells. Most of the cells get disintegrated and some of them undergo shrinkage which leads to early-stage apoptosis. Usually, the cancer cells appear as a chaotic collection of cells in an array of uneven shapes and sizes in the microscope; however, in normal cells, the nucleus has a smooth appearance and maintains a uniform, spheroid shape. After treating with ZnO NPs, some cells were floating, became rounder and smaller, and refraction also decreased; some cell debris was observed in the medium. The cells left on the wall became rounder and smaller (Fig. 8) [35–38]; however, it is noteworthy that when assessing the cell viability of SKMEL-28 cancer cells and normal cells

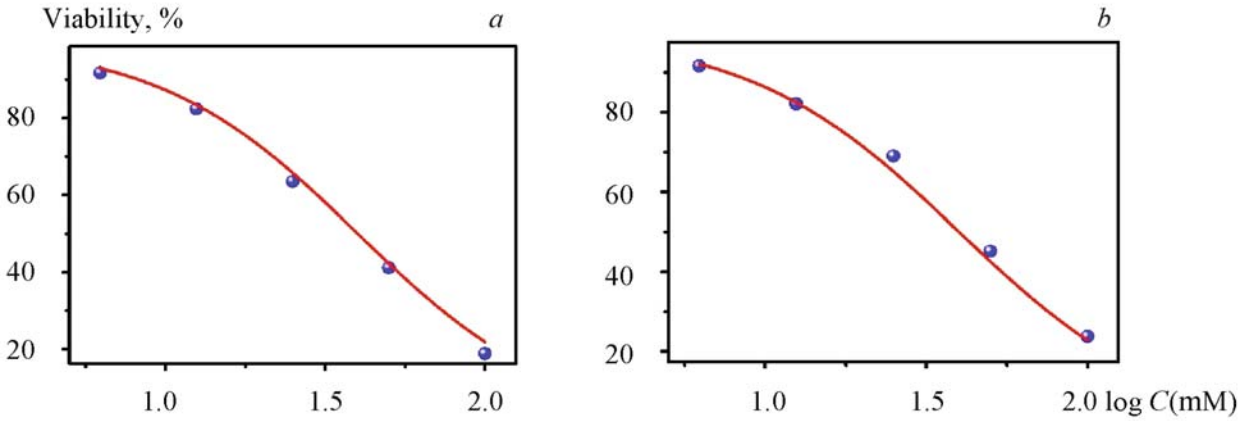

Fig. 7. Sigmoidal curve of ZnO NPs on (a) SKMEL-28 cell line and (b) L6 normal cell line.

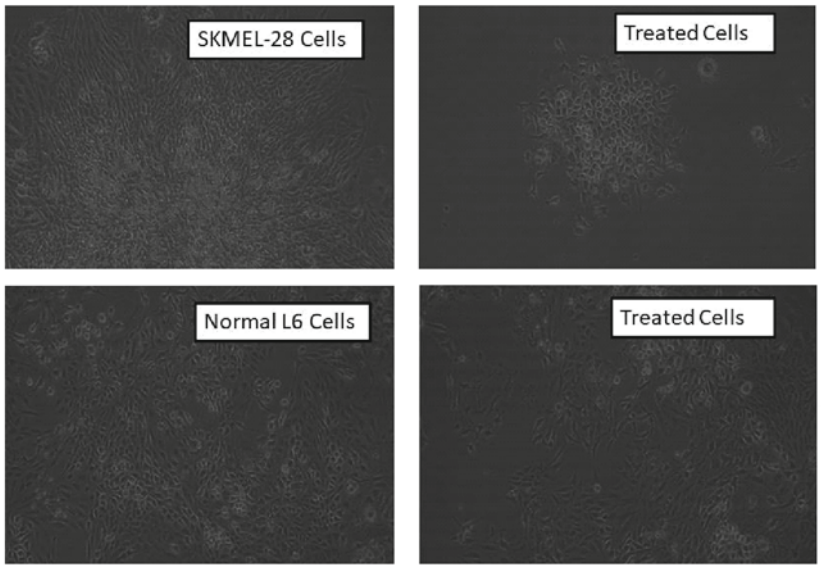

Fig. 8. Structural morphology of normal cells and treated cancer cells (cytotoxic effect of ZnO NPs on the SKMEL-28 cell line).

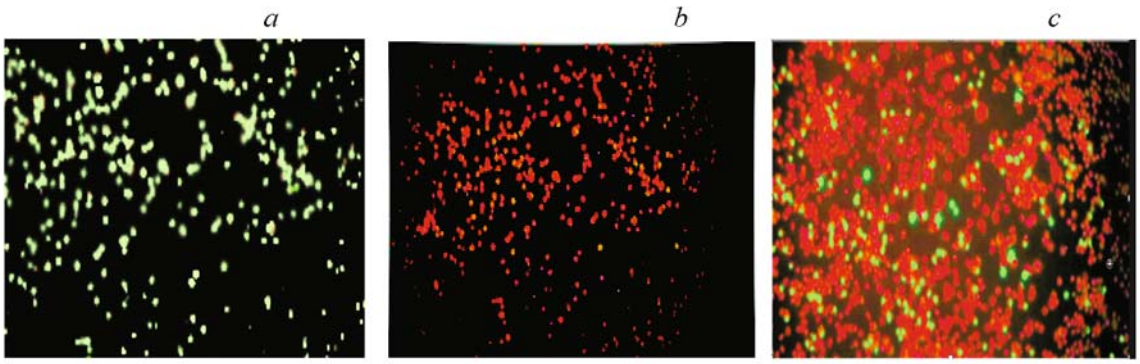

Fig. 9. AO/EB staining of the SKMEL-28 cell line.

exposed to ZnO NPs, the former exhibits a higher level of activity than the latter. This disparity arises from the fact that ZnO NPs affect the cancer cells while having a lesser impact on normal cells, as clearly depicted in Fig. 8. In the case of a normal cell line, ZnO NPs do not disrupt the living cells even after the treatment. Conversely, in the SKMEL-28 cell line, ZnO NPs break the cluster of cancer cells, leading to membrane blebbing, chromatin condensation and the early stages of apoptosis. These mechanisms are consistent with previous findings in the literature [39–42].

Furthermore, the cytotoxicity of ZnO NPs was confirmed by the AO/EB double staining method. The changes observed in this method were exhibited by fluorescent microscopic images. In the AO/EB double staining method, the green colour (Fig. 9a) shows living cells and the orange colour (Fig. 9b) denotes treated cells. Figure 9c shows that the cancer cells that are affected by the ZnO NPs, while not affecting normal cells. Hence, the changes that occur in AO/EB staining can be identified by chromatin condensation. This result shows the early and late apoptotic nature of ZnO NPs.

Conclusions. The current investigation unveils the ethanolic extract of Mangifera indica seeds as a sustainable and cost-effective resource for synthesizing ZnO NPs. The confirmation of ZnO NPs was achieved through UV-visible studies, revealing their absorption maxima. FT-IR analysis indicates distinctive absorption patterns in the fingerprint region below 1000 cm^{-1}, which could be attributed to interatomic vibrations, further validating the composition as metal oxides. XRD pattern demonstrated the crystalline nature of the particles, while SEM and TEM images affirmed their unique rice grain-like morphology. Moreover, EDAX provided crucial insights by detecting the presence of metal ions within the nanoparticles, corroborating the purity of the ZnO NPs by the absence of impurities or extraneous compounds. Notably, ZnO NPs exhibit remarkable potential as anti-cancer agents, particularly against the SKMEL-28 cell line, displaying an IC50 value of 32.686 μg/mL, in contrast to the 49.011 μg/mL observed in the L6 cell line. These findings align with observations of apoptotic activity within the cells, characterized by pronounced morphological changes and chromatin condensation, thus affirming the induction of both early and late apoptotic processes by ZnO NPs. This underscores their potential as a valuable tool in anti-cancer therapy.

REFERENCES

1. K. S. Bipinchandra, S. S. Shailesh, S. I. Lee, and B. S. Kim, *World J. Microbiol. Biotechnol*., **32**, 180 (2016).
2. K. Pramila, Y. Ravi Kumar, S. Deepak Kumar, K. Leeladhar Kanwar, and S. Sushil Kumar, *J. Nanostruct. Chem*., **8**, Article ID 217224 (2018).
3. Z. Guan, S. Ying, P. C. Ofoegbu, P. Clubb, C. Rico, F. He, and J. Hong, *Environ. Technol*. *Innov*., **26**, Article ID 102336 (2022).
4. M. Pellei, F. D. Bello, M. Porchia, and C. Santini, *Coord. Chem. Rev*., **445**, Article ID 214088 (2021).
5. S. M. Makiwa, M. N. Mthiyane, C. E. Anthony, M. Singh, and C. O. Damian, *Sci. Afr*., **17**, Article ID 01365 (2022).
6. A. M. Mousa, A. A. Hamid, A. Haggran, T. E. Zakia, A. E. Khier, S. M. Sabry, and S. E. Rashad, *Egypt. J. Chem*., **65**, No. 11, 122–128 (2022).
7. S. N. Mothersill, C. Mothersill, D. Sheehan, N. O. Brien, J. O. Halloran, F. N. A. M. Van Pelt, and M. Davoren, *Toxicol. Vitro*, **18**, No. 13, 365–376 (2004).
8. H. A. Alhadlaq, M. J. Akhtar, and M. Ahamed, *Cell Biosci*., **5**, No. 12, 9236–9282 (2015).
9. R. Sha, A. Basak, P. Chandra Maity, and S. Badhulika, *Sens. Actuat. Rep*., **4**, Article ID 100098 (2022).
10. A. M. Youssef and S. M. E. Sayed, *Carbohydr. Polym*., **193**, 19–27 (2018).
11. S. Ahmed, M. Ahmad, B. L. Swami, and S. Ikram, *J. Adv. Res*., **7**, No. 1, 17–28 (2016).
12. K. Lingaraju, H. Raja Naika, K. Manjunath, R. B. Basavaraj, H. Nagabhushana, G. Nagaraju, and D. Suresh, *Appl. Nanosci*., **6**, 703–710 (2016).
13. E. Zare, S. Pourseyedi, M. Khatami, and D. Esmaeel, *J. Mol. Struct*., **1146**, 96–103 (2017).
14. M. D. Jayappa, K. R. Chandrashekar, M. A. Pavan Kumar, D. Suresh, A. Prabhu, P. D. Rekha, and S. Sheikh, *Appl. Nanosci*., **10**, 3057–3074 (2020).
15. L. Gibot, S. Chabaud, S. Bouhout, S. Bolduc, F. A. Auger, and V. J. Moulin, *Int. J. Biolog*. *Macromol*., **72**, 370–379 (2015).
16. T. L. Cristian, R. Rojas, J. C. Contreras-Esquivel, L. Serna-Cock, R. E. Belmares-Cerda, and C. N. Aguilar, *Trends Food Sci. Technol*., **55**, 109–117 (2016).
17. M. Shahnaza, M. Danish, M. H. B. Ismail, M. T. Ansari, and M. N. M. Ibrahim, *Sustain. Chem. Pharma*, **14**, Article ID 100179 (2019).

18. C. O. Tettey and H. M. Shin, *Sci. Afr*., **157**, 321–324 (2019).
19. J. Santhosh Kumar, S. Venkat Kumar, and S. Rajesh Kumar, *Res. Eff. Technol*., **3**, 459–465 (2017).
20. J. Ali, R. Irshad, B. Li, K. Tahir, A. Ahmad, M. Shakeel, N. U. Khan, and Z. U. Khan, *J. Photochem. Photobiol. B: Biolog*., **183**, 349–356 (2018).
21. S. B. Ulaeto, G. M. Mathew, J. K. Pancrecious, J. B. Nair, T. P. D. Rajan, K. K. Maiti, and B. C. Pai, *ACS Biomater. Sci. Eng.*, **6**, No. 1, 235–245 (2020).
22. M. Bhat, B. Chakraborty, R. Suresh Kumar, A. I. Almansour, N. Arumugam, D. Kotresha, S. S. Pallavi, S. B. Dhanyakumara, K. N. Shashiraj, and S. Nayaka, *J. King Saud. Univ. Sci*., **2**, No. 33, Article ID 101296 (2021).
23. S. Bishnoi, A. Kumar, and R. Selvaraj, *Mater. Res. Bull*., **97**, 121–132 (2018).
24. C. Chinnasamy, P. Tamilselvam, B. Karthick, B. Sidharth, and M. Senthilnathan, *Mater. Today: Proc*., **5**, No. 2, 6728–6735 (2018).
25. N. Bala, S. Saha, M. Chakraborty, M. Maiti, S. Das, R. Basu, and P. Nandy, *RSC Adv*., **5**, 4993–5003 (2015).
26. P. Naresh Kumar, K. Sakthivel, and V. Balasubramanian, *Mater. Sci. Pol*., **35**, No. 1, 111–118 (2017).
27. P. R. Anupama, J. Garvasis, S. Sheera, K. Oruvil, and A. Joseph, *J. Phys. Chem. Solids*, **127**, 265–274 (2019).
28. R. K. Saha, M. K. Debanath, B. Paul, S. Medhi, and E. Saiki, *Sci. Rep*., **10**, 2598–2607 (2020).
29. G. Bisht and S. Rayamajhi, *Nanobiomed*. (*RIJ*), **3**, 9–16 (2016).
30. N. K. Kadiyala, B. K. Mandal, L. V. Kumar Reddy, C. H. Barnes, L. De Los Santos Valladares, and D. Sen, *ACS Omega*, **8**, No. 2, 2406–2420 (2023).
31. C. I. Sobanaraj and M. A. Princela, *Int. J. Sci. Tech. Res*., **8**, No. 9, 2189–2198 (2020).
32. J. Gomis-Tena, B. M. Brown, J. Cano, B. Trenor, P. C. Yang, J. Saiz, C. E. Clancy, and L. Romero, *J. Chem. Inf. Model*., **60**, No. 3, 1779–1790 (2020).
33. C. H. Ng, S. M. Kong, Y. L. Tiong, M. J. Maah, N. Sukram, M. Ahmad, and A. S. B. Khoo, *Metallomics*, **6**, No. 4, 892–906 (2014).
34. W. Berger, E. Hauptmann, L. Elbling, M. Vetterlein, E. M. Kokoschka, and M. Micksche, *Int. J. Cancer*, **71**, No. 1, 108–115 (1997).
35. D. D. Cui, Y. Huang, S. H. Mao, S. C. Chen, M. Qiu, L. L. Ji, and C. Yi, *Braz. J. Med. Biol. Res*., **42**, 854–862 (2009).
36. Z. Dang, J. Sun, J. Fan, J. Li, X. Li, and T. Chen, *Mater. Sci. Eng. C*, **124**, Article ID 112071 (2021).
37. M. Reimer and C. Zollfrank, *Adv. Energy Mater*., **11**, No. 43, Article ID 2003866 (2021).
38. X. Zhao, S. Zeng, H. Feng, Y. Wang, S. Li, X. Zhou, M. Wang, and L. Rei, *Int. J. Biol. Macromol*., **200**, 234–241 (2022).
39. S. Majeed, M. Danish, M. H. B. Ismail, M. T. Ansari, and M. N. M. Ibrahim, *Sustain. Chem. Pharm*., **14**, Article ID 100179 (2019).
40. F. Gao, N. Ma, H. Zhou, Q. Wang, H. Zhang, P. Wang, H. Hou, H. Wen, and L. Li, *Int. J. Nanomedicine*, 3859–3874 (**2016**).
41. M. Govarthanan, P. Srinivasan, T. Selvankumar, V. Janaki, F. A. Al-Misned, H. A. El-Serehy, W. Kim, and S. Kamala-Kannan, *Mater. Lett*., **273**, Article ID 127951 (2020).
42. M. J. Khan, A. Ahmad, M. A. Khan, and S. Siddiqui, *Biol. Trace Elem. Res*., **199**, 2172–2181 (2021).